PERGAMON

International Journal of Solids and Structures 40 (2003) 2321–2342

INTERNATIONAL JOURNAL OF SOLIDS and STRUCTURES

www.elsevier.com/locate/ijsolstr

The viscoelastic and viscoplastic behavior of low-density polyethylene

Aleksey D. Drozdov [a,*], Qiang Yuan [b]

[a] *Department of Chemical Engineering, West Virginia University, P.O. Box 6102 Morgantown, WV 26506, USA*
[b] *State Key Laboratory of Polymer Physics and Chemistry, Changchun Institute of Applied Chemistry, Chinese Academy of Sciences, Changchun 130022, China*

Received 25 December 2002; received in revised form 28 January 2003

Abstract

Three series of tensile tests with constant cross-head speeds (ranging from 5 to 200 mm/min), tensile relaxation tests (at strains from 0.03 to 0.09) and tensile creep tests (at stresses from 2.0 to 6.0 MPa) are performed on low-density polyethylene at room temperature. Constitutive equations are derived for the time-dependent response of semicrystalline polymers at isothermal deformation with small strains. A polymer is treated as an equivalent heterogeneous network of chains bridged by temporary junctions (entanglements, physical cross-links and lamellar blocks). The network is thought of as an ensemble of meso-regions linked with each other. The viscoelastic behavior of a polymer is modelled as thermally-induced rearrangement of strands (separation of active strands from temporary junctions and merging of dangling strands with the network). The viscoplastic response reflects mutual displacement of meso-domains driven by macro-strains. Stress–strain relations for uniaxial deformation are developed by using the laws of thermodynamics. The governing equations involve five material constants that are found by fitting the observations. Fair agreement is demonstrated between the experimental data and the results of numerical simulation. It is shown that observations in conventional creep tests reflect not only the viscoelastic, but also the viscoplastic behavior of an ensemble of meso-regions.

Keywords: Semicrystalline polymers; Low-density polyethylene; Viscoelasticity; Viscoplasticity

1. Introduction

This paper is concerned with the nonlinear viscoelastic and viscoplastic behavior of injection-molded low-density polyethylene (LDPE) in uniaxial tensile tests in the sub-yield region of deformations at room temperature. The nonlinear time-dependent response of polyethylene has been a focus of attention in the past decade, which may be explained by numerous industrial applications of this semicrystalline polymer. LDPE is used for production of bags, pallet covers and greenhouse films. Although pristine LDPE has

* Corresponding author. Tel.: +1-304-293-2111; fax: +1-304-293-4139.
E-mail address: aleksey.drozdov@mail.wvu.edu (A.D. Drozdov).

0020-7683/03/$ - see front matter © 2003 Elsevier Science Ltd. All rights reserved.
doi:10.1016/S0020-7683(03)00074-X

rather modest mechanical properties, they can be noticeably improved by mixing polyethylene with polypropylene, polystyrene, polyester, polyamides, as well as by reinforcing LDPE with carbon black and calcium carbonate. Polyethylene is also one of the key components for production of thermoplastic elastomers.

The nonlinear viscoelastic behavior of polyethylene is conventionally studied in standard creep and relaxation tests. Creep of polypropylene samples has recently been investigated by Lai and Bakker (1995), Suwanprateeb et al. (1995), Ward (1995), G'Sell et al. (1996), Rand et al. (1996), Zhang and Moore (1997), Deng et al. (1998), Lee and Pienkowski (1998), Zhou and Wilkes (1998), Bonner et al. (1999), Xu et al. (2000), Hubert et al. (2002), to mention a few. Experimental data in relaxation tests on polypropylene have recently been reported by Chengalva et al. (1995), Djokovic et al. (1999), Nitta and Suzuki (1999), Djokovic et al. (2000) and Meyer and Pruitt (2001).

Viscoplasticity and yielding of polyethylene with relation to its crystalline morphology and topology of chains have been studied in the past decade by Lu et al. (1995), Brooks et al. (1997, 1998, 1999a,b), Gaucher-Miri and Seguela (1997), Graham et al. (1997), Vaccaro et al. (1997), Butler and Donald (1998), Hiss et al. (1999), Sabbagh and Lesser (1999), Hobeika et al. (2000), Sirotkin and Brooks (2001), Bergström et al. (2002) and Seguela (2002).

Despite a number of publications focused on the mechanical response of polyethylene, some features of its time-dependent behavior remain obscure. First, most of previous studies were confined to one type of tests only [as exceptions, it is worth noting the works by Ward (1995), G'Sell et al. (1996) and Zhang and Moore (1997), where stress–strain curves in tensile tests with constant strain rates were compared with creep curves]. Second, no stress–strain relations have been developed in previous publications that can adequately describe both the viscoelastic and viscoplastic responses of semicrystalline polymers and whose adjustable parameters have transparent physical meaning. Finally, previous studies treated experimental data in creep and relaxation tests as two equivalent ways for the observation of the viscoelastic behavior of polymers. This approach was formulated about half a century ago with application to the *linear* time-dependent response of solid polymers (Ferry, 1980). In the past decades, however, this concept was used without revision to predict the *nonlinear* viscoelastic behavior of polymers in the sub-yield region of deformations.

The objective of this study is three-fold:

1. To report experimental data in tensile tests with constant strain rates, in tensile relaxation tests and in tensile creep tests on LDPE in the sub-yield region of deformations at ambient temperature.
2. To derive constitutive equations for the viscoelastic and viscoplastic behavior of a semi-crystalline polymer and to find adjustable parameters in the stress–strain relations by fitting the observations.
3. To demonstrate a pronounced difference between the time-dependent responses of LDPE in creep and relaxation tests. We suggest that the relaxation curves reflect merely the viscoelastic behavior of a semicrystalline polymer, whereas the creep curves in the sub-yield region of deformations reflect both the viscoelastic and viscoplastic responses.

To clarify the latter assertion, it should unambiguously formulated what we understand under the viscoelastic and viscoplastic phenomena in semicrystalline polymers.

LDPE is a semicrystalline polymer, where spherulites of various types are distributed in the amorphous matrix. The average radius of spherulites ranges from 3 to 12 μm (Graham et al., 1997). They contain crystalline lamellae with the thickness of 8–10 nm. The average size of lamellae and their curvature, as well as the type of their organization into spherulites are strongly affected by crystallization conditions, molecular weight, and the degree of branching of chains. At room temperature, the amorphous phase is in the rubbery state. The glass transition point of polyethylene remains the subject of debate (Badr et al., 2000; Shieh and Liu, 2001; Tanaka, 2001), but most authors agree that the glass transition temperature, T_g, is

located far below room temperature. The amorphous phase consists of chains located in inter-lamellar and inter-spherulitic regions with various levels of molecular mobility (Shieh and Liu, 2001). The crystalline morphology of polyethylene is strongly affected by deformation. Loading of LDPE in the sub-yield region of deformations results in (i) inter-lamellar separation, (ii) rotation and twist of lamellae, (iii) fine slip of lamellar blocks (homogeneous shear of layer-like crystalline structures), (iv) reorientation of lamellae within spherulites, (v) chain slip through the crystals, (vi) sliding of tie chains along and their detachment from lamellar blocks (Brooks et al., 1997; Gaucher-Miri and Seguela, 1997; Hiss et al., 1999; Seguela, 2002).

To develop constitutive equations for a semicrystalline polymer, we apply a method of homogenization (Bergström et al., 2002). According to this approach, a complicated micro-structure of a polymer is replaced by an equivalent phase, whose behavior captures essential features of the mechanical response. A heterogeneous network of chains bridged by temporary junctions (entanglements, physical cross-links on the surfaces of crystallites and lamellar blocks) is chosen as the equivalent phase for the following reasons: (i) the viscoelastic response is conventionally associated with rearrangement of chains in amorphous regions (Coulon et al., 1998), (ii) the viscoplastic flow is "initiated in the amorphous phase before transitioning into the crystalline phase" (Meyer and Pruitt, 2001), and (iii) sliding of tie chains along and their detachment from lamellar blocks play the key role in the yielding phenomenon (Nitta and Takayanagi, 1999).

The viscoelastic response of LDPE is described within the concept of transient networks (Green and Tobolsky, 1946; Yamamoto, 1956; Lodge, 1968; Tanaka and Edwards, 1992; Drozdov and Christiansen, 2002). It is modelled as separation of active strands from temporary junctions and merging of dangling strands with the network. The network of chains is assumed to be strongly heterogeneous, and it is treated as an ensemble of meso-regions (MRs) with various activation energies for detachment of active strands. Two types of MRs are distinguished: (i) active domains, where strands separate from junctions as they are thermally agitated (these MRs are associated with a mobile part of the amorphous phase), and (ii) passive domains where detachment of strands from their junctions is prevented (these MRs reflect a part of the amorphous phase whose mobility is severely restricted by surrounding crystallites). Rearrangement of active strands in the network is thought of as a thermally-activated process whose rate obeys the Eyring equation (Eyring, 1936).

The viscoplastic behavior of LDPE is described based on the concept of non-affine networks (Glatting et al., 1994; Wedgewood and Geurts, 1995; Sun et al., 2000). Under deformation, junctions slide with respect to their reference positions in a stress-free polymer. Sliding of junctions reflects sliding of chains with respect to entanglements, sliding of tie chains along the surfaces of crystallites, and fine slip of lamellar blocks. The sliding process occurs at arbitrary small stresses, which means that "there is no yield surface... and plastic deformation commences from the onset of loading, although it may be exceedingly small below certain levels of applied stress" (Lubarda and Benson, 2002). Unlike previous studies on non-affine networks, sliding of junctions between strands is connected with the macro-strain (not macro-stress). An advantage of this (merely kinetic) approach is that the unloaded configuration of a network may be determined explicitly, which is of essential importance for the analysis of residual strains induced by viscoplastic flow.

With reference to the above scenario for the viscoelastic and viscoplastic responses of semi-crystalline polymers, we associate observations in standard relaxation tests with the viscoelastic behavior (detachment of active strands from temporary junctions in a transient network, where the junctions remain at rest). On the contrary, observations in standard creep tests reflect the viscoelastic and viscoplastic behavior (rearrangement of strands in a network, where junctions slide with respect to their reference positions). At small stresses, when the viscoplastic flow of junctions is negligible, the time-dependent response in both tests is attributed to rearrangement of a network only, which implies that the experimental data may be recalculated by using conventional formulas. With an increase in stress (strain), when the viscoplastic flow of junctions becomes substantial, creep and relaxation tests reflect different processes as the micro-level.

The purpose of the remaining part of this paper is to validate this scenario. The exposition is organized as follows. The experimental procedure is described in Section 2. Kinematic equations for sliding of junctions are introduced in Section 3. Rearrangement of strands in a transient network is discussed in Section 4. The strain energy density of a semicrystalline polymer is determined is Section 5. Stress–strain relations for uniaxial deformation of a specimen are derived in Section 6 by using the laws of thermodynamics. Adjustable parameters in the constitutive equations are found in Section 7 by matching experimental data. Our findings are discussed in Section 8. Some concluding remarks are formulated in Section 9.

2. Experimental procedure

Low-density polyethylene (Lupolen 2410T) was supplied by BASF (Basell). ASTM dumbbell specimens were injection molded with length 148 mm, width 9.8 mm and thickness 3.8 mm. Uniaxial tensile tests were performed at room temperature on a testing machine Instron-5568 equipped with electro-mechanical sensors for the control of longitudinal strains in the active zone of samples (with a distance of 50 mm between clips). The tensile force was measured by a standard load cell. The longitudinal stress, σ, was determined as the ratio of the axial force to the cross-sectional area of stress-free specimens.

Mechanical tests were carried out on samples not subjected to thermal pre-treatment. To minimize the effect of physical aging, experiments were performed at least one day after preparation of samples. Each test was performed on a new specimen. Necking of samples was not observed.

In the first series of tests, specimens were loaded with constant cross-head speeds of 5, 10, 25, 50, 100, 150 and 200 mm/min (which corresponded to the strain rates $\dot{\epsilon} = 9.80 \times 10^{-4}$, 2.03×10^{-3}, 5.16×10^{-3}, 9.92×10^{-3}, 2.07×10^{-2}, 3.03×10^{-2} and 4.00×10^{-2} s^{-1}, respectively) up to the maximal strain $\epsilon_{max} = 0.1$. The maximal strain were chosen to be close to the yield strain for LDPE, $\epsilon_y = 0.12$ (Hobeika et al., 2000). The chosen strain rates ensured nearly isothermal experimental conditions, on the one hand, and they allowed the viscoelastic effects to be disregarded, on the other. The duration of tensile tests varied from 3.3 s at the highest cross-head speed to 132 s at the lowest one. Our observations in relaxation tests (see Fig. 2) demonstrated that during 132 s the maximal decrease in the longitudinal stress did not exceed 23%.

The engineering stress, σ, is plotted versus the engineering strain, ϵ, in Fig. 1. The stress–strain diagrams show that (i) the stress–strain curves are strongly nonlinear, and (ii) given a strain, ϵ, the stress, σ, monotonically increases with the strain rate.

Tensile relaxation tests were carried out at the longitudinal strains $\epsilon = 0.03$, 0.06, and 0.09 that cover the entire region of sub-yield deformations. In each relaxation test, a specimen was stretched with a constant cross-head speed of 25 mm/min up to a given longitudinal strain, ϵ, that was preserved constant during the relaxation time. In accord with the ASME protocol for short-term relaxation tests, the relaxation time $t_r = 20$ min was chosen.

The longitudinal stress, σ, is plotted versus the logarithm ($\log = \log_{10}$) of time t (the initial instant, $t = 0$, corresponds to the beginning of the relaxation process) in Fig. 2. This figure shows that given a strain, ϵ, the stress, σ, decreases (practically linearly) with the logarithm of time, t. Given time, t, the stress, σ, monotonically increases with the strain, ϵ, and the relaxation curves are similar to one another (in the sense that they may be superposed by shifts along the vertical axis with a high level of accuracy).

Tensile creep tests were performed at the longitudinal stresses $\sigma = 2.0$, 3.0, 4.0, 4.5, 5.0, 5.5 and 6.0 MPa. We confine ourselves to this interval of loads, because at higher stresses, the secondary and tertiary creep flows are observed within the experimental time-scale. The latter phenomena remain beyond the scope of the present study which focuses on the time-dependent response of LDPE at small strains.

In each creep test, a specimen was deformed with a constant cross-head speed of 50 mm/min up to a given longitudinal stress, σ, that was preserved constant during the creep time. Following the ASME protocol for short-term creep tests, the creep time, $t_c = 20$ min, was chosen.

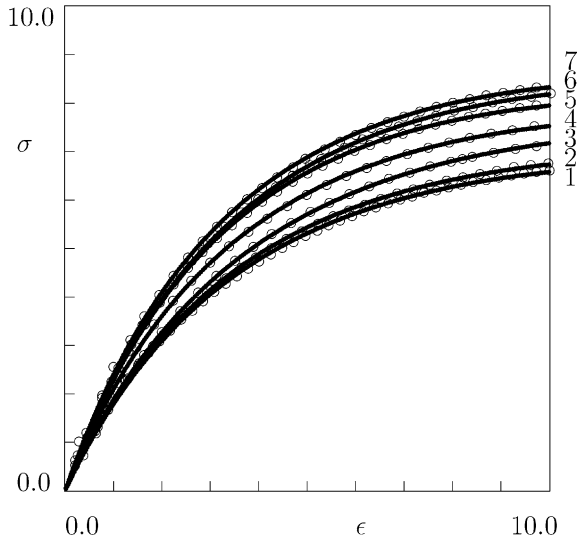

Fig. 1. The stress σ MPa versus strain ϵ in a tensile test with the cross-head speed u mm/min. Circles: experimental data. Solid lines: results of numerical simulation. Curve 1: $u = 5.0$. Curve 2: $u = 10.0$. Curve 3: $u = 25.0$. Curve 4: $u = 50.0$. Curve 5: $u = 100.0$. Curve 6: $u = 150.0$. Curve 7: $u = 200.0$.

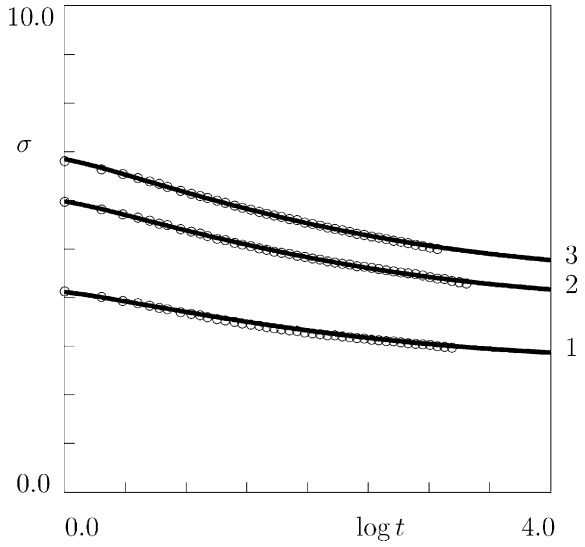

Fig. 2. The stress σ MPa versus time t s in a tensile relaxation test with a strain ϵ. Circles: experimental data. Solid lines: results of numerical simulation. Curve 1: $\epsilon = 0.03$. Curve 2: $\epsilon = 0.06$. Curve 3: $\epsilon = 0.09$.

The longitudinal strain, ϵ, is plotted versus the logarithm of time t (the initial instant, $t = 0$, corresponds to the beginning of the creep process) in Fig. 3. This figure shows that given a stress, σ, the strain, ϵ, monotonically increases with time, t. The growth of rather weak at relatively small stresses, and its rate noticeably increases with stress. Unlike the relaxation curves (Fig. 2) that can be fairly well superposed by

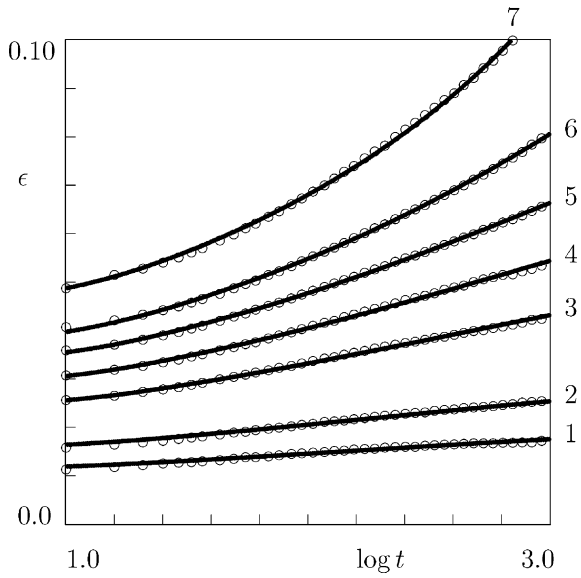

Fig. 3. The strain ϵ versus time t s in a tensile creep test with a stress σ MPa. Circles: experimental data. Solid lines: results of numerical simulation. Curve 1: $\sigma = 2.0$. Curve 2: $\sigma = 3.0$. Curve 3: $\sigma = 4.0$. Curve 4: $\sigma = 4.5$. Curve 5: $\sigma = 5.0$. Curve 6: $\sigma = 5.5$. Curve 7: $\sigma = 6.0$.

shifts along the vertical axis, no superposition of the creep curves (Fig. 3) is possible by vertical shifts. Given time, t, the strain, ϵ, monotonically increases with the stress, σ.

Our aim now is to develop constitutive equations that can correctly describe the experimental data depicted in Figs. 1–3.

3. Non-affine deformation

A semicrystalline polymer is treated as a heterogeneous network of strands bridged by temporary junctions. The spatial heterogeneity of the network is attributed to an inhomogeneity of interactions between chains in the amorphous phase and crystalline lamellae with various lengths and thicknesses. The network is thought of as an ensemble of MRs with arbitrary shapes and sizes. The characteristic length of a MR substantially exceeds the radius of gyration for a macromolecule, and it is noticeably less than the characteristic size of a sample.

Straining of a specimen in the sub-yield region of deformations induces sliding of junctions between strands with respect to their reference positions. Sliding of junctions in meso-domains of an equivalent network reflects

1. sliding of entanglements in the amorphous phase,
2. slippage of tie chains along lamellar surfaces,
3. fine slip of crystalline lamellae (homogeneous shearing of layer-like crystallites).

Sliding of junctions is characterized by a plastic strain ϵ_p. MRs in an ensemble are connected with one another by links (lamellar blocks) that transmit macro-deformation to individual MRs. This implies that

the macro-strain, ϵ, equals the sum of the elastic strain in MRs ϵ_e (the elastic strain is supposed to be the same for all meso-domains) and the plastic strain ϵ_p,

$$\epsilon = \epsilon_e + \epsilon_p. \tag{1}$$

The rate of non-affine deformation of the network, $\dot{\epsilon}_p = d\epsilon_p/dt$, is assumed to be proportional to the rate of macro-strain, $\dot{\epsilon} = d\epsilon/dt$,

$$\frac{d\epsilon_p}{dt}(t) = \alpha(\epsilon_e(t))\frac{d\epsilon}{dt}(t). \tag{2}$$

The coefficient of proportionality, α, is treated as a function of the elastic strain, ϵ_e. This coefficient vanishes at the zero elastic strain, monotonically increases with ϵ_e, and tends to unity at relatively large deformations (the latter means that the rate of sliding for a developed flow of junctions coincides with the rate of macro-strain).

The evolution of the coefficient α is described by the first-order kinetic equation

$$\frac{d\alpha}{d\epsilon_e}(\epsilon_e) = \frac{1}{\varepsilon}[1 - \alpha(\epsilon_e)],$$

where ε stands for the strain that characterizes transition to the steady viscoplastic flow. Integration of this equation with the initial condition $\alpha(0) = 0$ implies that

$$\alpha(\epsilon_e) = 1 - \exp\left(-\frac{\epsilon_e}{\varepsilon}\right). \tag{3}$$

Eqs. (1)–(3) describe non-affine deformation of an equivalent network of chains that reflects the viscoplastic response of a semicrystalline polymer.

4. Rearrangement of strands

The viscoelastic behavior of a polymer is modelled within the concept of transient networks. Active strands (whose ends are connected to contiguous junctions) are assumed to separate from temporary junctions at random times when these strands are thermally activated. An active strand whose end detaches from a junction is transformed into a dangling strand. A dangling strand returns into the active state when its free end captures a nearby junction at a random instant.

Two types of MRs in an ensemble are distinguished: passive and active. In passive MRs, inter-chain interaction prevents detachment of strands from the network, which implies that all junctions in these domains are permanent. In active MRs, active strands separate from temporary junctions and dangling strands merge with the network at random times.

Denote by X_a be the number of active strands in active MRs, by X_p the number of strands connected to the network in passive MRs, and by X the average number of active strands per unit mass of a polymer. These quantities are assumed (i) to be independent of mechanical factors, and (ii) to obey the conservation law

$$X_a + X_p = X. \tag{4}$$

Separation of active strands from their junctions and merging of dangling strands with the network are thought of as thermally activated processes. Detachment of active strands from their junctions is governed by the Eyring equation, where different meso-domains are characterized by different activation energies, ω, for separation of strands. According to the theory of thermally-activated processes (Eyring, 1936), the rate of detachment for an active strand in a MR with activation energy ω is given by

$$\Gamma = \Gamma_0 \exp\left(-\frac{\omega}{k_B T}\right),$$

where k_B is Boltzmann's constant, T is the absolute temperature, and the pre-factor, Γ_0, is independent of energy, ω, and temperature, T. Sliding of junctions in a non-affine network with respect to their reference positions does not affect the attempt rate, Γ_0, and the activation energy of a MR, ω. In what follows, we confine ourselves to isothermal deformations at a reference temperature, T_0. Introducing the dimensionless activation energy

$$v = \frac{\omega}{k_B T_0},$$

we find that

$$\Gamma(v) = \Gamma_0 \exp(-v). \tag{5}$$

Active MRs with various dimensionless activation energies, v, are characterized by the distribution function, $p(v)$, that equals the ratio of the number, $N_a(v)$, of active strands in active meso-domains with energy v to the total number of active strands, X_a,

$$N_a(v) = X_a p(v). \tag{6}$$

The distribution function, $p(v)$, is independent of mechanical factors.

The kinetics of rearrangement of an ensemble of active meso-domains is entirely determined by the function $n_a(t,\tau,v)$ that equals the number of active strands at time t (per unit mass) belonging to active MRs with activation energy v that have last rearranged before instant $\tau \in [0,t]$. In particular, $n_a(t,t,v)$ is the number (per unit mass) of active strands in active MRs with activation energy v in the deformed medium at time t,

$$n_a(t,t,v) = N_a(v). \tag{7}$$

The amount $\varphi(\tau,v)\,d\tau$, where

$$\varphi(\tau,v) = \frac{\partial n_a}{\partial \tau}(t,\tau,v)\bigg|_{t=\tau}, \tag{8}$$

equals the number (per unit mass) of dangling strands in active MRs with activation energy v that merge with the network within the interval $[\tau,\tau+d\tau]$, and the quantity

$$\frac{\partial n_a}{\partial \tau}(t,\tau,v)\,d\tau$$

is the number of these strands that have not detached from their junctions during the interval $[\tau,t]$. The number (per unit mass) of strands in active MRs that separate (for the first time) from the network within the interval $[t,t+dt]$ reads

$$-\frac{\partial n_a}{\partial t}(t,0,v)\,dt,$$

whereas the number (per unit mass) of strands in active MRs that merged with the network during the interval $[\tau,\tau+d\tau]$ and, afterwards, separated from the network within the interval $[t,t+dt]$ is given by

$$-\frac{\partial^2 n_a}{\partial t\,\partial \tau}(t,\tau,v)\,dt\,d\tau.$$

The rate of detachment, Γ, equals the ratio of the number of active strands that separate from the network per unit time to the current number of active strands. It follows from this definition that the evolution of the

function $n_a(t,0,v)$, that equals the number (per unit mass) of active strands that detach (for the first time) from temporary junctions within the interval $[t,t+dt]$, is governed by the equation

$$\frac{\partial n_a}{\partial t}(t,0,v) = -\Gamma(v) n_a(t,0,v). \tag{9}$$

Applying this definition to active strands that merged with the network during the interval $[\tau,\tau+d\tau]$ and separate from temporary junctions within the interval $[t,t+dt]$, we find that

$$\frac{\partial^2 n_a}{\partial t\,\partial \tau}(t,\tau,v) = -\Gamma(v)\frac{\partial n_a}{\partial \tau}(t,\tau,v). \tag{10}$$

The solutions of Eqs. (9) and (10) with initial conditions (7) and (8) read

$$n_a(t,0,v) = N_a(v)\exp[-\Gamma(v)t], \tag{11}$$

$$\frac{\partial n_a}{\partial \tau}(t,\tau,v) = \varphi(\tau,v)\exp[-\Gamma(v)(t-\tau)]. \tag{12}$$

To determine the function $\varphi(t,v)$, we use the identity

$$n_a(t,t,v) = n_a(t,0,v) + \int_0^t \frac{\partial n_a}{\partial \tau}(t,\tau,v)\,d\tau,$$

which, together with Eq. (7), implies that

$$n_a(t,0,v) + \int_0^t \frac{\partial n_a}{\partial \tau}(t,\tau,v)\,d\tau = N_a(v). \tag{13}$$

Differentiating Eq. (13) with respect to time and using Eq. (12), we obtain

$$\varphi(t,v) + \frac{\partial n_a}{\partial t}(t,0,v) + \int_0^t \frac{\partial^2 n_a}{\partial t\,\partial \tau}(t,\tau,v)\,d\tau = 0.$$

This equality together with Eqs. (9), (10) and (13) results in

$$\varphi(t,v) = \Gamma(v) N_a(v).$$

Substitution of this expression into Eq. (12) implies that

$$\frac{\partial n_a}{\partial \tau}(t,\tau,v) = \Gamma(v) N_a(v)\exp[-\Gamma(v)(t-\tau)]. \tag{14}$$

Introducing the concentration of active MRs,

$$\kappa = \frac{X_a}{X},$$

and substituting Eq. (6) into Eqs. (11) and (14), we arrive at the formulas

$$\begin{aligned} n_a(t,0,v) &= \kappa X p(v)\exp[-\Gamma(v)t], \\ \frac{\partial n_a}{\partial \tau}(t,\tau,v) &= \kappa X p(v)\Gamma(v)\exp[-\Gamma(v)(t-\tau)], \end{aligned} \tag{15}$$

which describe rearrangement of active strands in an equivalent transient network.

5. The strain energy density

A strand is modelled as a linear elastic medium with the mechanical energy

$$w = \tfrac{1}{2}\mu e^2,$$

where μ is the average rigidity per strand and e is the strain from the stress-free state to the deformed state.

For strands belonging to passive meso-domains, the strain, e, coincides with the elastic strain, ϵ_e. Multiplying the strain energy per strand by the number of strands in passive MRs, we find the mechanical energy of meso-domains where rearrangement of strands is prevented by surrounding macromolecules,

$$W_p(t) = \tfrac{1}{2}\mu X_p \epsilon_e^2(t). \tag{16}$$

With reference to the conventional theory of temporary networks (Tanaka and Edwards, 1992), stresses in dangling strands are assumed to totally relax before these strands merge with the network. This implies that the reference (stress-free) state of a strand that merges with the network at time τ coincides with the deformed state of the network at that instant. For active strands that have not rearranged until time t, the strain, $e(t)$, coincides with $\epsilon_e(t)$, whereas for active strands that have last merged with the network at time $\tau \in [0,t]$, the strain, $e(t,\tau)$, is given by

$$e(t,\tau) = \epsilon_e(t) - \epsilon_e(\tau).$$

Summing the strain energies of active strands belonging to active MRs with various activation energies, v, that rearranged at various instants, $\tau \in [0,t]$, we find the mechanical energy of active meso-domains,

$$W_a(t) = \frac{1}{2}\mu \int_0^\infty \mathrm{d}v \left\{ n_a(t,0,v)\epsilon_e^2(t) + \int_0^t \frac{\partial n_a}{\partial \tau}(t,\tau,v)[\epsilon_e(t) - \epsilon_e(\tau)]^2 \,\mathrm{d}\tau \right\}. \tag{17}$$

The mechanical energy per unit mass of a polymer reads

$$W(t) = W_a(t) + W_p(t).$$

Substitution of expressions (1), (16) and (17) into this equality implies that

$$W(t) = \frac{1}{2}\mu \left\{ X_p(\epsilon(t) - \epsilon_p(t))^2 + \int_0^\infty \mathrm{d}v \left[n_a(t,0,v)(\epsilon(t) - \epsilon_p(t))^2 + \int_0^t \frac{\partial n_a}{\partial \tau}(t,\tau,v)((\epsilon(t) - \epsilon_p(t)) - (\epsilon(\tau) - \epsilon_p(\tau)))^2 \,\mathrm{d}\tau \right] \right\}. \tag{18}$$

Differentiation of Eq. (18) with respect to time results in

$$\frac{\mathrm{d}W}{\mathrm{d}t}(t) = \mu A(t)\left[\frac{\mathrm{d}\epsilon}{\mathrm{d}t}(t) - \frac{\mathrm{d}\epsilon_p}{\mathrm{d}t}(t)\right] - \frac{1}{2}\mu A_0(t), \tag{19}$$

where

$$A(t) = X_p(\epsilon(t) - \epsilon_p(t)) + \int_0^\infty \mathrm{d}v \left\{ n_a(t,0,v)(\epsilon(t) - \epsilon_p(t)) + \int_0^t \frac{\partial n_a}{\partial \tau}(t,\tau,v)\big[(\epsilon(t) - \epsilon_p(t)) - (\epsilon(\tau) - \epsilon_p(\tau))\big]\mathrm{d}\tau \right\}, \tag{20}$$

$$A_0(t) = -\int_0^\infty \mathrm{d}v \left\{ \frac{\partial n_a}{\partial t}(t,0,v)(\epsilon(t) - \epsilon_p(t))^2 + \int_0^t \frac{\partial^2 n_a}{\partial t \partial \tau}(t,\tau,v)\big[(\epsilon(t) - \epsilon_p(t)) - (\epsilon(\tau) - \epsilon_p(\tau))\big]^2 \mathrm{d}\tau \right\}. \tag{21}$$

It follows from Eqs. (1), (2) and (19) that

$$\frac{\mathrm{d}W}{\mathrm{d}t}(t) = \mu A(t)\big[1 - \alpha(\epsilon(t) - \epsilon_{\mathrm{p}}(t))\big]\frac{\mathrm{d}\epsilon}{\mathrm{d}t}(t) - \frac{1}{2}\mu A_0(t). \tag{22}$$

Bearing in mind Eqs. (6) and (13), we transform Eq. (20) as follows:

$$A(t) = \left[X_{\mathrm{p}} + X_{\mathrm{a}}\int_0^\infty p(v)\,\mathrm{d}v\right](\epsilon(t) - \epsilon_{\mathrm{p}}(t)) - \int_0^\infty \mathrm{d}v\int_0^t \frac{\partial n_{\mathrm{a}}}{\partial\tau}(t,\tau,v)(\epsilon(\tau) - \epsilon_{\mathrm{p}}(\tau))\,\mathrm{d}\tau.$$

This formula together with Eq. (4) and the equality

$$\int_0^\infty p(v)\,\mathrm{d}v = 1 \tag{23}$$

implies that

$$A(t) = X(\epsilon(t) - \epsilon_{\mathrm{p}}(t)) - \int_0^\infty \mathrm{d}v\int_0^t \frac{\partial n_{\mathrm{a}}}{\partial\tau}(t,\tau,v)(\epsilon(\tau) - \epsilon_{\mathrm{p}}(\tau))\,\mathrm{d}\tau. \tag{24}$$

Substitution of expressions (9) and (10) into Eq. (21) results in

$$A_0(t) = \int_0^\infty \Gamma(v)\,\mathrm{d}v\left\{n_{\mathrm{a}}(t,0,v)(\epsilon(t) - \epsilon_{\mathrm{p}}(t))^2 + \int_0^t \frac{\partial n_{\mathrm{a}}}{\partial\tau}(t,\tau,v)\big[(\epsilon(t) - \epsilon_{\mathrm{p}}(t)) - (\epsilon(\tau) - \epsilon_{\mathrm{p}}(\tau))\big]^2\mathrm{d}\tau\right\}. \tag{25}$$

Our aim now is to apply Eqs. (22), (24) and (25) in order to derive stress–strain relations for a semicrystalline polymer.

6. Constitutive equations

For uniaxial deformation of a non-affine transient network at a reference temperature, T_0, the Clausius–Duhem inequality reads

$$T_0\frac{\mathrm{d}Q}{\mathrm{d}t}(t) = -\frac{\mathrm{d}W}{\mathrm{d}t}(t) + \frac{1}{\rho}\sigma(t)\frac{\mathrm{d}\epsilon}{\mathrm{d}t}(t) \geqslant 0, \tag{26}$$

where ρ is density, and Q is entropy production per unit mass. Substitution of expression (22) into Eq. (26) implies that

$$T_0\frac{\mathrm{d}Q}{\mathrm{d}t}(t) = \frac{1}{\rho}[\sigma(t) - \rho\mu A(t)(1 - \alpha(\epsilon(t) - \epsilon_{\mathrm{p}}(t)))]\frac{\mathrm{d}\epsilon}{\mathrm{d}t}(t) + \frac{1}{2}\mu A_0(t) \geqslant 0. \tag{27}$$

It follows from Eq. (25) that the function $A_0(t)$ is non-negative: $\Gamma(v)$ is positive as the rate of rearrangement of strands, whereas $n_{\mathrm{a}}(t,0,v)$ and $\partial n_{\mathrm{a}}(t,\tau,v)/\partial\tau$ are non-negative as concentrations of active strands in active MRs. This means that dissipation inequality (27) is satisfied for an arbitrary deformation program, $\epsilon = \epsilon(t)$, provided that the expression in the square brackets vanishes. This assertion together with Eqs. (15) and (24) results in the stress–strain relation

$$\sigma(t) = E\left[1 - \alpha\left(\epsilon(t) - \epsilon_{\mathrm{p}}(t)\right)\right]\left\{[\epsilon(t) - \epsilon_{\mathrm{p}}(t)] - \kappa\int_0^\infty p(v)\,\mathrm{d}v\int_0^t \Gamma(v)\exp[-\Gamma(v)(t-\tau)][\epsilon(\tau) - \epsilon_{\mathrm{p}}(\tau)]\,\mathrm{d}\tau\right\}, \tag{28}$$

where $E = \rho\mu X$ is an analog of Young's modulus.

The time-dependent response of a semicrystalline polymer at isothermal uniaxial deformation with small strains is determined by Eqs. (1)–(3), (5) and (28). Our purpose now is to study three cases of interest for applications, when the governing equations can be substantially simplified.

(1) We begin with uniaxial tension with a relatively large strain rate, when the viscoelastic effects may be disregarded during the loading period. Neglecting the integral term in Eq. (28), we find that

$$\sigma(t) = E[1 - \alpha(\epsilon(t) - \epsilon_p(t))][\epsilon(t) - \epsilon_p(t)]. \tag{29}$$

The stress–strain relation (29) differs from conventional constitutive equations in viscoplasticity by the first term in square brackets. Given a deformation program, $\epsilon(t)$, Eqs. (1)–(3) and (29) are determined by two adjustable parameters:

1. the elastic modulus E,
2. the strain, ε, that characterizes transition to the steady viscoplastic flow.

(2) We analyze now a standard relaxation test with a longitudinal strain ϵ,

$$\epsilon(t) = \begin{cases} 0, & t < 0, \\ \epsilon, & t \geqslant 0. \end{cases} \tag{30}$$

It follows from Eqs. (2) and (30) that the plastic strain, ϵ_p, remains constant during the relaxation test. It equals the plastic strain, $\epsilon_p(\epsilon)$, reached along the loading path of the stress–strain curve. Substitution of expressions (5) and (30) into Eq. (28) implies that

$$\sigma(t, \epsilon) = \sigma_0(\epsilon)\left\{1 - \kappa \int_0^\infty [1 - \exp(-\Gamma_0 t \exp(-v))] p(v)\, dv\right\}, \tag{31}$$

where

$$\sigma_0(\epsilon) = E[1 - \alpha(\epsilon - \epsilon_p(\epsilon))](\epsilon - \epsilon_p(\epsilon))$$

is the longitudinal stress at the beginning of the relaxation test.

To fit experimental data, we adopt the random energy model (Derrida, 1980) with the quasi-Gaussian distribution function,

$$p(v) = p_0 \exp\left[-\frac{(v - V)^2}{2\Sigma^2}\right] \quad (v \geqslant 0), \qquad p(v) = 0 \quad (v < 0), \tag{32}$$

where V and Σ are adjustable parameters, and the pre-factor p_0 is determined by condition (23).

Given a strain ϵ, the time-dependent response of a semicrystalline polymer in relaxation test (30) is determined by Eqs. (31) and (32). As the material parameters, Γ_0 and V, in these equations are mutually dependent (an increase in Γ_0 results in an increase in V), we set $\Gamma_0 = 1\ s^{-1}$ without loss of generality. After this simplification, Eqs. (31) and (32) involve three material constants:

1. the average activation energy for rearrangement of strands V,
2. the standard deviation of activation energies Σ,
3. the concentration of active MRs κ.

The stress at the beginning of the relaxation test, σ_0, is found by integration of Eqs. (1)–(3) and (29) along the loading path of the stress–strain curve.

(3) We study now a standard creep test with a longitudinal stress σ,

$$\sigma(t) = \begin{cases} 0, & t < 0, \\ \sigma, & t \geqslant 0. \end{cases} \tag{33}$$

It follows from Eqs. (1), (28) and (33) that the elastic strain, $\epsilon_e(t)$, is given by

$$\epsilon_e(t) = \frac{\sigma}{E[1-\alpha(\epsilon_e(t))]} + \kappa \int_0^\infty Z(t,v)p(v)\,dv, \tag{34}$$

where

$$Z(t,v) = \int_0^t \Gamma(v)\exp[-\Gamma(v)(t-\tau)]\epsilon_e(\tau)\,d\tau.$$

Bearing in mind Eq. (5), we find that the function $Z(t,v)$ satisfies the differential equation

$$\frac{\partial Z}{\partial t}(t,v) = \Gamma_0 \exp(-v)[\epsilon_e(t) - Z(t,v)], \quad Z(0,v) = 0. \tag{35}$$

After the elastic strain, $\epsilon_e(t)$, has been determined from Eqs. (34) and (35), the macro-strain, $\epsilon(t)$, is found from Eqs. (1) and (2), which imply that

$$\frac{d\epsilon}{dt}(t) = \frac{1}{1-\alpha(\epsilon_e(t))}\frac{d\epsilon_e}{dt}(t). \tag{36}$$

Given a stress, σ, Eqs. (3) and (34)–(36) involve five material constants: E, ε, V, Σ and κ that can be found by fitting observations in tensile tests with constant strain rates and in relaxation tests. The initial strain, $\epsilon(0)$, and the initial elastic strain, $\epsilon_e(0)$, are determined by integration of Eqs. (1)–(3) and (29) along the loading path of the stress–strain curve.

Summing up these results, we conclude that constitutive equations (1)–(3), (5) and (28) can describe the time-dependent behavior of a semicrystalline polymer in conventional quasi-static tests. The model involves five adjustable parameters, which is substantially less than the number of material constants in other stress–strain relations for solid polymers (Hasan and Boyce, 1995; Buckley et al., 1996; Spathis and Kontou, 1998; Boyce et al., 2000; Ho and Krempl, 2000; Bergström et al., 2002). An advantage of the governing equations is that the adjustable parameters have transparent physical meaning. Our aim now is to find the experimental constants by matching the observations depicted in Figs. 1–3.

7. Fitting of observations

We begin with matching the stress–strain diagrams depicted in Fig. 1. It follows from Eqs. (1)–(3) and (29) that

$$\begin{aligned} &\sigma(\epsilon) = E(\epsilon-\epsilon_p)\exp\Big(-\frac{\epsilon-\epsilon_p}{\varepsilon}\Big), \\ &\frac{d\epsilon_p}{d\epsilon}(\epsilon) = 1-\exp\Big(-\frac{\epsilon-\epsilon_p}{\varepsilon}\Big), \quad \epsilon_p(0) = 0. \end{aligned} \tag{37}$$

To find the quantities, E and ε, we fix an interval $[0, \varepsilon_{max}]$, where the "best-fit" parameter, ε, is assumed to be located, and divide this interval into J subintervals by the points $\varepsilon^{(i)} = i\Delta\varepsilon$ $(i = 1, \ldots, J)$ with $\Delta\varepsilon = \varepsilon_{max}/J$. Given $\varepsilon^{(i)}$, Eqs. (37) are integrated numerically by the Runge–Kutta method with the step $\Delta\epsilon = 1.0 \times 10^{-5}$. The elastic modulus, E, is found by the least-squares method from the condition of minimum of the function

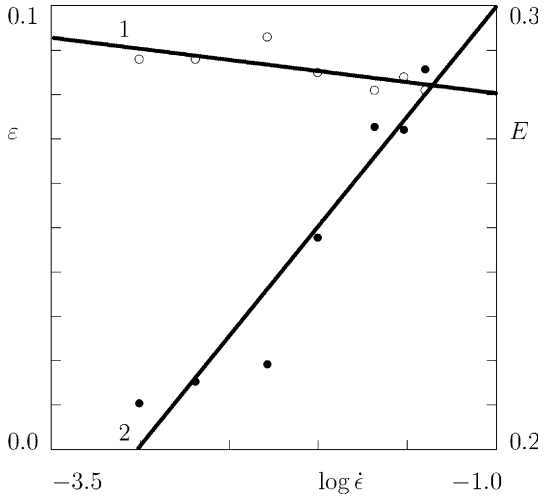

Fig. 4. The strain ε (unfilled circles) and Young's modulus E GPa (filled circles) versus the strain rate $\dot{\epsilon}$ s^{-1}. Symbols: treatment of observations in tensile tests. Solid lines: approximation of the experimental data by Eqs. (38). Curve 1: $\varepsilon_0 = 7.528 \times 10^{-2}$, $\varepsilon_1 = 5.007 \times 10^{-3}$. Curve 2: $E_0 = 3.491 \times 10^{-1}$, $E_1 = 4.940 \times 10^{-2}$.

$$F = \sum_{\epsilon_m} [\sigma_{\exp}(\epsilon_m) - \sigma_{\text{num}}(\epsilon_m)]^2,$$

where the sum is calculated over all experimental points, ϵ_m, on a stress–strain curve, $\sigma_{\exp}$ is the stress measured in a tensile test, and σ_{num} is given by Eqs. (37). The "best-fit" parameter, ε, is determined from the condition of minimum of the function F. After determining the "best-fit" value, $\varepsilon^{(i)}$, this procedure is repeated twice for the new intervals, $[\varepsilon^{(i-1)}, \varepsilon^{(i+1)}]$, to ensure good accuracy of fitting.

Fig. 1 demonstrates excellent agreement between the observations and the results of numerical simulation. The adjustable parameters, E and ε, are plotted in Fig. 4 versus the strain rate, $\dot{\epsilon}$. The experimental data are approximated by the functions

$$E = E_0 + E_1 \log \dot{\epsilon}, \quad \varepsilon = \varepsilon_0 - \varepsilon_1 \log \dot{\epsilon}, \tag{38}$$

where the coefficients, E_m and ε_m $(m = 0, 1)$, are determined by the least-squares algorithm. Fig. 4 shows that Eqs. (38) correctly describe the effect of strain rate on Young's modulus, E, and the strain for transition to a developed flow of junctions, ε.

Relations (38) are chosen to match the experimental data, because the first equality in Eqs. (38) is conventionally employed to assess the effect of strain rate on elastic moduli. It should be noted, however, that Eqs. (38) cannot correctly predict the influence of strain rate on E and ε at relatively low strain rates (which is typical of creep tests). According to Eqs. (38), at small values of $\dot{\epsilon}$, Young's modulus becomes negative, whereas the strain for transition to a steady flow of junctions approaches infinity. To adequately describe changes in the Young modulus, E, and the strain, ε, at relatively small strain rates, the following phenomenological equations are proposed:

$$E = E_0(1 + \tau_{\text{E}}\dot{\epsilon})^n, \quad \varepsilon = \varepsilon_\infty + \frac{\varepsilon_0 - \varepsilon_\infty}{(1 + \tau_\varepsilon \dot{\epsilon})^2}, \tag{39}$$

where E_0 is Young's modulus at infinitesimaly small strain rates, ε_0 and ε_∞ are strains for transition to a developed flow of junctions at small and large strain rates, respectively, n is a dimensionless exponent, and τ_{E} and τ_ε are characteristic times. The first equality in Eqs. (39) is similar to the Carreau B model, while the

other equality is analogous to the Carreau A model for the effect of strain rate on the viscosity of polymer fluids. An advantage of Eqs. (39) is that they predict finite values of E and ε at small strain rates. A shortcoming of these equations is that Eqs. (39) involve six adjustable parameters compared to four material constants in Eqs. (38).

The adjustable parameters in Eqs. (39) are determined by the nonlinear regression algorithm. Fig. 5 demonstrates fair agreement between the experimental data and the results of numerical simulation.

We proceed with fitting the relaxation curves depicted in Fig. 2 by Eqs. (31) and (32) with $\Gamma_0 = 1\ \mathrm{s}^{-1}$. First, we fit the relaxation curve at $\epsilon = 0.06$. The experimental data are determined by four experimental constants: V, Σ, κ and σ_0. To determine these quantities, we fix the intervals $[0, V_{\max}]$ and $[0, \Sigma_{\max}]$, where the "best-fit" parameters, V and Σ, are assumed to be located, and divide these intervals into J subintervals by the points $V^{(i)} = i\Delta V$ and $\Sigma^{(j)} = j\Delta\Sigma$ $(i, j = 1, \ldots, J)$ with $\Delta V = V_{\max}/J$ and $\Delta\Sigma = \Sigma_{\max}/J$. For any pair, $\{V^{(i)}, \Sigma^{(j)}\}$, the integral in Eq. (31) is evaluated numerically by Simpson's method with 200 points and the step $\Delta v = 0.15$. The pre-factor p_0 in Eq. (32) is determined from Eq. (23). The coefficients κ and σ_0 are found by the least-squares algorithm from the condition of minimum of the function

$$F = \sum_{t_m} [\sigma_{\exp}(t_m) - \sigma_{\mathrm{num}}(t_m)]^2,$$

where the sum is calculated over all experimental points t_m, depicted in Fig. 2, the stress, $\sigma_{\exp}$, is measured in the relaxation test, and the stress, σ_{num}, is given by Eq. (31). The "best-fit" parameters, V and Σ, minimize the function F on the set $\{V^{(i)}, \Sigma^{(j)}\}$.

To approximate relaxation curves at other strains, ϵ, we fix the constants, V, Σ and κ, found by matching the experimental data at $\epsilon = 0.06$ and fit each relaxation curve by using the only adjustable parameter, the initial stress, $\sigma_0(\epsilon)$. This quantity is determined by the least-squares algorithm from the condition of minimum of the function F. Fig. 2 demonstrates good agreement between the observations in all relaxation tests and the results of numerical analysis.

The initial stresses, σ_0, found by matching the experimental data in relaxation tests are plotted versus the corresponding strains, ϵ, in Fig. 6. In this figure, we also present observations in the tensile test with the cross-head speed 25 mm/min (that coincides with the cross-head speed for the loading paths in the relaxation tests)

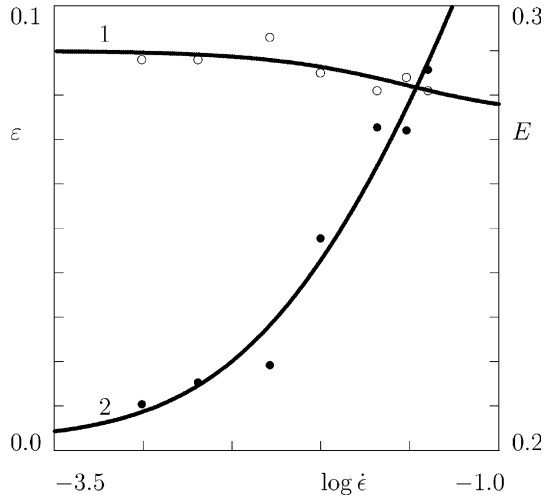

Fig. 5. The strain ε (unfilled circles) and Young's modulus E GPa (filled circles) versus the strain rate $\dot{\epsilon}\ \mathrm{s}^{-1}$. Symbols: treatment of observations in tensile tests. Solid lines: approximation of the experimental data by Eqs. (39). Curve 1: $\varepsilon_0 = 8.999 \times 10^{-2}$, $\varepsilon_\infty = 7.586 \times 10^{-2}$, $\tau_\varepsilon = 16.2$ s. Curve 2: $E_0 = 0.202$ GPa, $\tau_{\mathrm{E}} = 251.0$ s, $n = 0.147$.

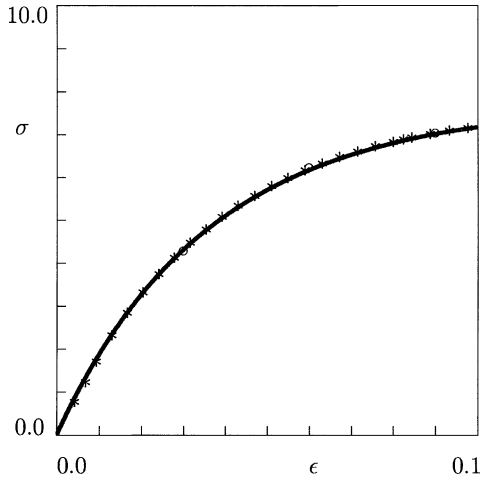

Fig. 6. The stress σ MPa versus strain ϵ. Asterisks: experimental data in a tensile test with the strain rate $\dot{\epsilon} = 5.2 \times 10^{-3}$ s^{-1}. Solid line: results of numerical simulation. Circles: treatment of observations in relaxation tests.

and the approximation of the experimental data in the tensile test by Eqs. (37). Fig. 6 reveals excellent agreement between the stresses, σ_0, determined by matching the observations in relaxation tests and the results of numerical analysis of the tensile test with the constant strain rate.

Finally, we match the experimental data in creep tests depicted in Fig. 3. In the fitting procedure, we use the adjustable parameters $V = 0.0$, $\Sigma = 6.0$ and $\kappa = 0.37$ determined by matching observations in tensile relaxation tests and the value $\varepsilon = 0.09$ that ensures the best prediction of the strain, ε, for transition to a developed flow of junctions at low strain rates ($\dot{\epsilon} = 0$) based on phenomenological relations (39).

To exclude Young's modulus, E, from the consideration, we present Eqs. (3) and (34)–(36) as follows:

$$\begin{aligned}
&\epsilon_{\rm e}(t) = \epsilon_{\rm e0}(\sigma)\exp\left(\frac{\epsilon_{\rm e}(t) - \epsilon_{\rm e0}(\sigma)}{\varepsilon}\right) + \kappa\int_0^\infty Z(t,v)p(v)\,{\rm d}v,\\
&\frac{\partial Z}{\partial t}(t,v) = \exp(-v)[\epsilon_{\rm e}(t) - Z(t,v)], \quad Z(0,v) = 0,\\
&\frac{{\rm d}\epsilon}{{\rm d}t}(t) = \exp\left(\frac{\epsilon_{\rm e}(t)}{\varepsilon}\right)\frac{{\rm d}\epsilon_{\rm e}}{{\rm d}t}(t), \quad \epsilon(0) = \epsilon_0(\sigma).
\end{aligned} \tag{40}$$

We take into account in these equations that $\Gamma_0 = 1$ s^{-1}.

For any stress, σ, integro-differential equations (40) involve two adjustable parameters: the initial strain, $\epsilon_0(\sigma)$, and the initial plastic strain, $\epsilon_{\rm p0}(\sigma)$. Each creep curve is matched independently. To find the constants, $\epsilon_0(\sigma)$ and $\epsilon_{\rm p0}(\sigma)$, we use an algorithm similar to that employed in the approximation of the experimental data in relaxation tests. We fix some intervals $[0, \epsilon_{\max}]$ and $[0, \epsilon_{\rm p\,max}]$, where the "best-fit" parameters, ϵ_0 and $\epsilon_{\rm p0}$, are assumed to be located, and divide these intervals into J subintervals by the points $e^{(i)} = i\Delta e$ and $e_{\rm p}^{(j)} = j\Delta e_{\rm p}$ $(i, j = 1, \ldots, J)$ with $\Delta e = \epsilon_{\max}/J$ and $\Delta e_{\rm p} = \epsilon_{\rm p\,max}/J$. For any pair, $\{e^{(i)}, e_{\rm p}^{(j)}\}$, Eqs. (32) and (40) are integrated numerically with the time step $\Delta t = 0.01$ and the initial conditions, $\epsilon_0 = e^{(i)}$ and $\epsilon_{\rm e0} = e^{(i)} - e_{\rm p}^{(j)}$, that follow from Eq. (1). The integral in Eqs. (40) is evaluated numerically by Simpson's method with the step $\Delta v = 0.15$. The "best-fit" quantities, ϵ_0 and $\epsilon_{\rm p0}$, are found from the condition of minimum of the function

$$F = \sum_{t_m} [\epsilon_{\exp}(t_m) - \epsilon_{\text{num}}(t_m)]^2,$$

where the sum is calculated over all experimental points t_m, depicted in Fig. 3, the strain, $\epsilon_{\exp}$, is measured in a creep test, and the strain, ϵ_{num}, is given by Eqs. (40). Fig. 3 reveals good agreement between the observations in creep tests and the results of numerical simulation.

The initial strain, ϵ_0, is plotted versus stress, σ, in Fig. 7. To compare results of numerical simulation in tensile creep tests and in tensile tests with a constant strain rate, we also present the observations in the tensile test with the cross-head speed 50 mm/min that corresponds to the loading paths of the creep curves. Fig. 7 demonstrates excellent agreement between the initial strains in the creep tests and the stress–strain curve for the tensile test.

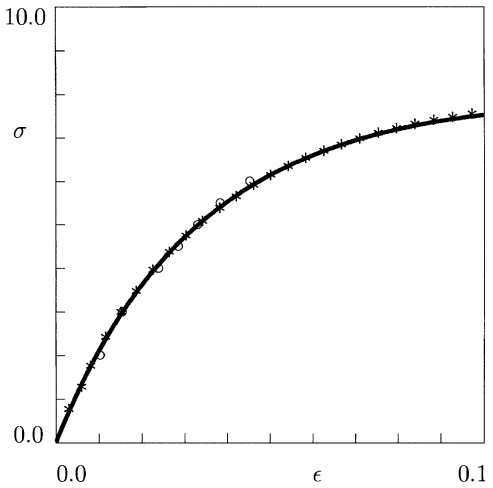

Fig. 7. The stress σ MPa versus strain ϵ. Asterisks: experimental data in a tensile test with the strain rate $\dot{\epsilon} = 9.9 \times 10^{-3}$ s^{-1}. Solid line: results of numerical simulation. Circles: treatment of observations in creep tests.

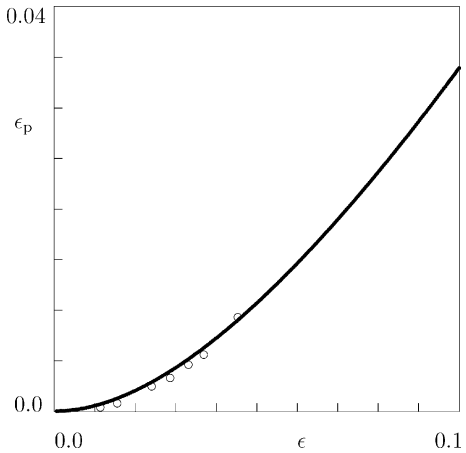

Fig. 8. The viscoplastic strain ϵ_p versus strain ϵ. Solid line: results of numerical simulation for a tensile test with the strain rate $\dot{\epsilon} = 9.9 \times 10^{-3}$ s^{-1}. Circles: treatment of observations in creep tests.

The initial plastic strain, ϵ_{p0}, is plotted versus the initial strain, ϵ_0, in Fig. 8 (circles). In this figure, the plastic strain, ϵ_p, is also depicted as a function of strain ϵ (solid line). The dependence of the plastic strain on the macro-strain is obtained by integration of Eqs. (37) with the adjustable parameters for the tensile test with the cross-head speed 50 mm/min. Fig. 8 shows fair agreement between the plastic strain, ϵ_p, determined in the approximation of observations in the tensile test, on the one hand, and that found by fitting the experimental data in the creep tests, on the other.

8. Discussion

Figs. 1–3 demonstrate that constitutive model (1)–(3), (28) and (32) correctly approximates the experimental data on LDPE in tensile tests with constant strain rates, as well as in tensile relaxation and creep tests at room temperature. We conclude from this observation that these stress–strain relations may be employed to describe the nonlinear time-dependent behavior of semicrystalline polymers in the sub-yield region of deformations.

Comparison of Eqs. (31) and (32) for the relaxation tests and Eqs. (32) and (34)–(36) for the creep tests reveals a substantial difference in the mechanical response of LDPE. The time-dependent behavior of the semicrystalline polymer in a relaxation test is merely viscoelastic (in the sense that the plastic strain, ϵ_p, remains constant during the test), whereas its behavior in a creep test reflects both the viscoelastic and viscoplastic responses (treated as detachment and attachment of strands from temporary junctions and sliding of junctions with respect to their reference positions, respectively). At relatively small strains, when the plastic deformation is negligible (the initial part of the curve depicted in Fig. 8), the time-dependent behavior of LDPE in both tests may be attributed to rearrangement of strands exclusively, which implies that experimental data in one test may be re-calculated into data in the other experiment by using conventional formulas (Ferry, 1980). With an increase in stress (strain), the plastic strain, ϵ_p, noticeably grows with time in a creep test, whereas this quantity remains constant in a relaxation test. This implies that observations in these two tests reflect different mechanisms for micro-deformation, and they cannot be re-calculated by using standard relations. This conclusion is confirmed by the experimental data presented in Figs. 2 and 3. These figures show that the relaxation curves can be fairly well superposed by vertical shifts (in terms of conventional models in viscoelasticity, this means that the relaxation spectrum is independent of strains), while the creep curves do not allow superposition by vertical shifts (which implies that the retardation spectra are strongly affected by stresses).

Figs. 4 and 5 show that the strain, ε, that characterizes transition to a steady flow of junctions decreases with the strain rate, $\dot{\epsilon}$. The reduction in ε is rather modest (about 8%), and it may be attributed to the rate-dependent rupture of tie chains (that bridge amorphous regions with crystalline lamellae), which enhances non-affine flow of junctions in the amorphous phase and fine slip of lamellar blocks in the crystalline phase.

According to Figs. 4 and 5, Young's modulus, E, substantially increases with the strain rate (by about 36%). This increase (driven by a reduction in the loading time from 132 to 3 s) cannot be associated with the viscoelastic response of LDPE only. The experimental data in relaxation tests (Fig. 2) demonstrate that the decrease in stress during this period (about 2 min) does not exceed 14%. To explain our findings, we refer to the concept of occluded rubber (Witten et al., 1993). According to this approach, part of amorphous regions in a virgin specimen are not deformed after application of external loads, because their deformation is severely restricted (screened) by surrounding lamellar blocks. Under stretching with relatively high strain rates, the lamellar blocks restricting mobility of occluded amorphous domains are disintegrated, and tie chains are broken that link amorphous regions with restricted mobility with surrounding crystallites. The larger the strain rate is, the more pronounced is damage of a crystalline structure, and, as a consequence, the higher is the amount of occluded amorphous domains to which macro-deformation is transmitted by their surroundings. This means that the number of active strands per unit mass of a polymer, X, grows with

the strain rate. As the elastic modulus, E, is proportional to X, we attribute the difference between the increase in Young's modulus observed in tensile tests with various strain rates and that observed in relaxation tests to the release of occluded amorphous regions induced by rate-dependent fragmentation of lamellar blocks. To account for this phenomenon in the constitutive equations, it suffices to treat E as a function of strain rate and to employ phenomenological relation (39) for the description of this dependence.

In the fitting procedure, we treated the initial strains, $\epsilon_0(\sigma)$, $\epsilon_{p0}(\sigma)$, and the initial stress, $\sigma_0(\epsilon)$, as adjustable parameters. After these parameters were found by matching the observations in creep and relaxation tests, we compared them with the same parameters determined in the approximation of the stress–strain curves in tensile tests with constants strain rates. The striking similarity of their values (Figs. 6–8) implies the conclusion about consistency of the constitutive model (in the sense that the values of material constants are independent of the tests in which they are determined). One can ask why we did not use the values of $\epsilon_0(\sigma)$, $\epsilon_{p0}(\sigma)$ and $\sigma_0(\epsilon)$ found in the approximation of stress–strain diagrams directly, but treated them as adjustable parameters in fitting creep and relaxation curves. Two answers may be provided. First, due to small discrepancies in their values for different specimens, the use of initial stresses and strains from the stress–strain curves will result in systematic deviations between the experimental data in creep and relaxation tests and the results of numerical simulation. Second, due to inertia of the testing machine, we expected some reduction in the plastic strain, ϵ_{p0}, at transition from the loading path of a stress–strain curve to a creep curve. This decrease in plastic strain has been previously observed in reverse creep tests on semicrystalline polymers, when a specimen was loaded with a constant strain rate up to a maximal strain, retracted with the same strain rate down to the zero stress, and the residual strain was measured as a function of time after unloading (Kitagawa et al., 1995; Ho and Krempl, 2000). A small (but systematic) decrease in the plastic strain is confirmed by the experimental data presented in Fig. 8. Fortunately, this decrease is rather insignificant, which implies that it may be neglected in the numerical analysis.

9. Concluding remarks

Three series of tensile tests with constant strain rates, tensile relaxation tests and tensile creep tests have been performed on injection-molded LDPE in the sub-yield region of deformations at room temperature.

Constitutive equations have been derived for the time-dependent behavior of semicrystalline polymers at isothermal deformation with small strains. A polymer is treated as an equivalent transient network of chains bridged by junctions (physical cross-links, entanglements and lamellar blocks). The heterogeneous network is thought of as an ensemble of MRs with various activation energies for separation of strands from temporary junctions.

The viscoelastic response reflects separation of active strands from temporary junctions in active meso-domains and merging of dangling strands with the network. Rearrangement of active strands is modelled as a thermally activated process whose rate is governed by the Eyring formula with the attempt rate and the activation energy independent of mechanical factors.

The viscoplastic response is attributed to sliding of junctions in a non-affine network with respect to their reference positions. The rate of sliding is proportional to the rate of macro-strain.

Stress–strain relations are derived by using the laws of thermodynamics. These equations involve five adjustable parameters that are determined by fitting the experimental data. Fair agreement is demonstrated between the observations and the results of numerical simulation.

It is shown that standard relaxation tests in the sub-yield region of deformations reflect the viscoelastic behavior of an ensemble of meso-domains at the micro-level, whereas the standard creep tests reflect both the viscoelastic and viscoplastic behavior of semicrystalline polymers.

The following conclusions are drawn:

1. The elastic modulus, E, noticeably grows with the strain rate, $\dot{\epsilon}$. This increase is attributed to fragmentation of lamellar blocks, breakage of tie chains and release of occluded amorphous regions, whose mobility is severely restricted by surrounding crystallites.
2. The strain, ε, that characterizes transition to a developed flow of junctions weakly decreases with the strain rate. This reduction in ε is associated with rate-dependent rupture of tie chains that enhances non-affine flow of junctions in the amorphous phase and fine slip of lamellar blocks.

Acknowledgements

A part of this work was performed when both authors visited Aalborg University (Denmark). The authors would like to express their sincere gratitude to the Department of Production (AU) for its hospitality.

References

Badr, Y., Ali, Z.I., Khafagy, R.M., 2000. On the mechanism of low temperature glass transition in low density polyethylene films. Radiation Physics and Chemistry 58, 87–100.

Bergström, J.S., Kurtz, S.M., Rimnac, C.M., Edidin, A.A., 2002. Constitutive modeling of ultra-high molecular weight polyethylene under large-deformation and cyclic conditions. Biomaterials 23, 2329–2343.

Bonner, M., Duckett, R.A., Ward, I.M., 1999. The creep behaviour of isotropic polyethylene. Journal of Materials Science 34, 1885–1898.

Boyce, M.C., Socrate, S., Llana, P.G., 2000. Constitutive model for the finite deformation stress-strain behavior of poly(ethylene terephthalate) above the glass transition. Polymer 41, 2183–2201.

Brooks, N.W., Unwin, A.P., Duckett, R.A., Ward, I.M., 1997. Temperature and strain rate dependence of yield strain and deformation behavior in polyethylene. Journal of Polymer Science. Part B: Polymer Physics 35, 545–552.

Brooks, N.W.J., Duckett, R.A., Ward, I.M., 1998. Temperature and strain-rate dependence of yield stress of polyethylene. Journal of Polymer Science. Part B: Polymer Physics 36, 2177–2190.

Brooks, N.W.J., Duckett, R.A., Ward, I.M., 1999a. Effects of crystallinity and stress state on the yield strain of polyethylene. Polymer 40, 7367–7372.

Brooks, N.W., Ghazali, M., Duckett, R.A., Unwin, A.P., Ward, I.M., 1999b. Effects of morphology on the yield stress of polyethylene. Polymer 40, 821–825.

Buckley, C.P., Jones, D.P., Jones, D.C., 1996. Hot-drawing of poly(ethylene terephthalate) under biaxial stress: application of a three-dimensional glass-rubber constitutive model. Polymer 37, 2403–2414.

Butler, M.F., Donald, A.M., 1998. A real-time simulteneous small- and wide-angle X-ray scattering study of in situ polyethylene deformation at elevated temperatures. Macromolecules 31, 6234–6249.

Chengalva, M.K., Kenner, V.H., Popelar, C.H., 1995. An evaluation of a free volume representation for viscoelastic properties. International Journal of Solids and Structures 32, 847–856.

Coulon, G., Castelein, G., G'Sell, C., 1998. Scanning force microscopic investigation of plasticity and damage mechanisms in polypropylene spherulites under simple shear. Polymer 40, 95–110.

Deng, M., Latour, R.A., Ogale, A.A., Shalaby, S.W., 1998. Study of creep behavior of ultra-high-molecular-weight polyethylene systems. Journal of Biomedical Materials Research 40, 214–223.

Derrida, B., 1980. Random-energy model: limit of a family of disordered models. Physical Review Letters 45, 79–92.

Djokovic, V., Kostoski, D., Galovic, S., Dramicanin, M.D., Kacarevic-Popovic, Z., 1999. Influence of orientation and irradiation on stress relaxation of linear low-density polyethylene (LLDPE): a two-process model. Polymer 40, 2631–2638.

Djokovic, V., Dramicanin, M.D., Kostoski, D., Dudic, D., 2000. Viscoelastic properties of polyethylene at elevated temperatures on the basis of two-process model for stress relaxation. Materials Science Forum 352, 195–200.

Drozdov, A.D., Christiansen, J. de C., 2002. The effect of annealing on the time-dependent behavior of isotactic polypropylene at finite strains. Polymer 43, 4745–4761.

Eyring, H., 1936. Viscosity, plasticity, and diffusion as examples of absolute reaction rates. Journal of Chemical Physics 4, 283–291.

Ferry, J.D., 1980. Viscoelastic Properties of Polymers. Wiley, New York.
Gaucher-Miri, V., Seguela, R., 1997. Tensile yield of polyethylene and related copolymers: mechanical and structural evidences of two thermally activated processes. Macromolecules 30, 1158–1167.
Glatting, G., Winkler, R.G., Reineker, P., 1994. Analytical model of the microscopic non-affine deformation of polymer networks. Journal of Chemical Physics 101, 2532–2538.
Graham, J.T., Alamo, R.G., Mandelkern, L., 1997. The effect of molecular weight and crystallite structure on yielding in ethylene copolymers. Journal of Polymer Science. Part B: Polymer Physics 35, 213–223.
Green, M.S., Tobolsky, A.V., 1946. A new approach to the theory of relaxing polymeric media. Journal of Chemical Physics 14, 80–92.
G'Sell, C., Dahoun, A., Hiver, J.M., Poinsot, C., 1996. Creep and yield behaviour of semi-crystalline polyethylene in uniaxial tension. Solid Mechanics and Its Applications 46, 75–82.
Hasan, O.A., Boyce, M.C., 1995. A constitutive model for the nonlinear viscoelastic viscoplastic behavior of glassy polymers. Polymer Engineering and Science 35, 331–344.
Hiss, R., Hobeika, S., Lynn, C., Strobl, G., 1999. Network stretching, slip processes, and fragmentation of crystallites during uniaxial drawing of polyethylene and related copolymers. A comparative study. Macromolecules 32, 4390–4403.
Ho, K., Krempl, E., 2000. Modeling of positive, negative and zero rate sensitivity by using the viscoplasticity theory based on overstress VBO. Mechanics of Time Dependent Materials 4, 21–42.
Hobeika, S., Men, Y., Strobl, G., 2000. Temperature and strain rate independence of critical strains in polyethylene and poly(ethylene-*co*-vinyl acetate). Macromolecules 33, 1827–1833.
Hubert, L., David, L., Seguela, R., Vigier, G., Corfias-Zuccalli, C., Germain, Y., 2002. Physical and mechanical properties of polyethylene for pipes in relation to molecular architecture. 2. Short-term creep of isotropic and drawn materials. Journal of Applied Polymer Science 84, 2308–2317.
Kitagawa, M., Zhou, D., Qiu, J., 1995. Stress–strain curves for solid polymers. Polymer Engineering and Science 35, 1725–1732.
Lai, J., Bakker, A., 1995. Analysis of the non-linear creep of high-density polyethylene. Polymer 36, 93–99.
Lee, K.-Y., Pienkowski, D., 1998. Compressive creep characteristics of extruded ultrahigh-molecular-weight polyethylene. Journal of Biomedical Materials Research 39, 261–265.
Lodge, A.S., 1968. Constitutive equations from molecular network theories for polymer solutions. Rheologica Acta 7, 379–392.
Lu, X., Qian, R., Brown, N., 1995. The effect of crystallinity on fracture and yielding of polyethylenes. Polymer 36, 4239–4244.
Lubarda, V.A., Benson, D.J., 2002. On the evolution equation for the rest stress in rate-dependent plasticity. International Journal of Plasticity 18, 895–918.
Meyer, R.W., Pruitt, L.A., 2001. The effect of cyclic true strain on the morphology, structure, and relaxation behavior of ultra high molecular weight polyethylene. Polymer 42, 5293–5306.
Nitta, K., Suzuki, K., 1999. Prediction of stress-relaxation behavior in high density polyethylene solids. Macromolecular Theory and Simulations 8, 254–259.
Nitta, K.-H., Takayanagi, M., 1999. Role of tie molecules in the yielding deformation of isotactic polypropylene. Journal of Polymer Science. Part B: Polymer Physics 37, 357–368.
Rand, J.L., Henderson, J.K., Grant, D.A., 1996. Nonlinear behavior of linear low-density polyethylene. Polymer Engineering and Science 36, 1058–1064.
Sabbagh, A.B., Lesser, A.J., 1999. On the phenomena of deformation and neck formation in LLDPE films subjected to uniaxial and biaxial loading conditions. Journal of Polymer Science. Part B: Polymer Physics 37, 2651–2663.
Seguela, R., 2002. Dislocation approach to the plastic deformation of semicrystalline polymers: kinetic aspects for polyethylene and polypropylene. Journal of Polymer Science. Part B: Polymer Physics 40, 593–601.
Shieh, Y.-T., Liu, C.-M., 2001. Phase segregation behavior in PE/DOP blends and glass-transition temperatures of polyethylene. Journal of Applied Polymer Science 82, 3591–3601.
Sirotkin, R.O., Brooks, N.W., 2001. The effects of morphology on the yield behaviour of polyethylene copolymers. Polymer 42, 3791–3797.
Spathis, G., Kontou, E., 1998. Experimental and theoretical description of the plastic behaviour of semicrystalline polymers. Polymer 39, 135–142.
Sun, N., Fong, C.F., De Kee, D., 2000. A non-affine transient network model. Rheologica Acta 39, 174–179.
Suwanprateeb, J., Tanner, K.E., Turner, S., Bonfield, W., 1995. Creep in polyethylene and hydroxyapatite reinforced polyethylene composites. Journal of Materials Science: Materials in Medicine 6, 804–807.
Tanaka, N., 2001. Characteristics of glass transition in propylene/ethylene copolymers and polyethylene. Thermochimica Acta 374, 1–5.
Tanaka, F., Edwards, S.F., 1992. Viscoelastic properties of physically cross-linked networks. Transient network theory. Macromolecules 25, 1516–1523.
Vaccaro, E., DiBenedetto, A.T., Huang, S.J., 1997. Yield strength of low-density polyethylene–polypropylene blends. Journal of Applied Polymer Science 63, 275–281.
Ward, I.M., 1995. Creep and yield behaviour of polyethylene. Macromolecular Symposia 98, 1029.

Wedgewood, L.E., Geurts, K.R., 1995. A non-affine network model for polymer melts. Rheologica Acta 34, 196–208.
Witten, T.A., Rubinstein, M., Colby, R.H., 1993. Reinforcement of rubber by fractal aggregates. Journal of Physics II France 3, 367–383.
Xu, B., Simonsen, J., Rochefort, W.E., 2000. Mechanical properties and creep resistance in polystyrene/polyethylene blends. Journal of Applied Polymer Science 76, 1100–1108.
Yamamoto, M., 1956. The visco-elastic properties of network structure. 1. General formalism. Journal of the Physical Society of Japan 11, 413–421.
Zhang, C., Moore, I.D., 1997. Nonlinear mechanical response of high density polyethylene. 1. Experimental investigation and model evaluation. Polymer Engineering and Science 37, 404–420.
Zhou, H., Wilkes, G.L., 1998. Creep behaviour of high density polyethylene films having well-defined morphologies of stacked lamellae with and without an observable row-nucleated fibril structure. Polymer 39, 3597–3609.